Research Article

Pulsatile Flow of Copper Suspended Nanofluid Venture Through a Bifurcated Artery

Gade Madhava Rao [*1] [iD], D. Srinivasacharya[2] [iD], I. Sreenath[1] [iD] and V. S. Bhagavan[3] [iD]

[1] *Department of Mathematics, Malla Reddy University, Hyderabad 500100, Telangana, India*
[2] *Department of Mathematics, National Institute of Technology, Warangal 506004, Telangana, India*
[3] *Department of Mathematics, Koneru Lakshmaiah Education Foundation, Vaddeswaram, Guntur 522502, Andhra Pradesh, India*

Abstract. With an aim to investigate the pulsatile flow of blood through a bifurcated artery with mild stenosis in the parent lumen in the manifestation of heat transmission. The blood is treated to be copper suspended nanofluid. The arteries forming bifurcation are assumed to be symmetric about the axis of the parent artery and straight circular cylinders of limited length. The highly nonlinear momentum and energy equations of nanofluid model are simplified by considering the mild stenosis case and a radial coordinate transformation is initiated to map irregular geometry into a rectangular grid. The solution for flow rate, impedance, shear stress are found by using the finite difference scheme in a cylindrical coordinate system. An extensive quantitative analysis has been performed based on numerical computations in order to estimate the effects of pertinent parameters on various physical quantities near the apex by means of their graphical representations so as to validate the applicability of the proposed mathematical model.

Keywords. Pulsatele blood flow, Copper nanoparticles, Bifurcated artery, Heat source parameter

Mathematics Subject Classification (2020). 76A05; 74S20

1. Introduction

For last couple of decades, researchers have become interested to model the blood flow in stenosed arteries experimentally and theoretically because it contributes an observation into physiological situations. The blood can be treated as a Newtonian or a non-Newtonian fluid,

---
[*]**Corresponding author:** rao.gmr.madhav@gmail.com

which ever the case may be considered. The formation of fatty materials like calcium on the inner wall of the artery, leads to abnormal and unnatural growth of the artery termed as stenosis and which may occur at various locations of the cardiovascular system. As the growth of the stenosis progress into lumen of the artery, blood flow will be reduced. So there is a relation between development of stenosis and the blood flow in the artery. The initiation of formation of stenosis is more likely to be dependent on the geometry of the artery like curvatures, junctions and bifurcations of large and medium arteries. The blood flow characteristics in the arterial system mainly depends on the attributes of the blood such as, viscosity, non-Newtonian character, size and shape of the artery and also the behavior of the flow like laminar or turbulent, pulsatile, micro-rotation etc. If development of stenosis takes a severe form, it may lead to stroke, heart attack and various cardiovascular diseases. Hence, the meticulous knowledge of the blood flow in a stenosed bifurcated artery may help in appropriate understanding and prevention of arterial diseases. Many investigators have been studying on physiological properties of blood flow through arterial system. Young [16] investigated the effect of development of mild stenosis in the lumen of the artery which is axially symmetric and time-dependent, whose cross section is constant through which a Newtonian fluid is flowing. The variations of shear stress with height of the stenosis, bifurcated angle and time both in coronary and femoral arteries near the flow divider has been presented by Shaw *et al.* [13]. Srinivasacharya and Srikanth [15] reported that the stenosis of the artery extremely changes the blood flow patterns in side the artery. Akbar [2] demonstrated the blood flow analysis of Prandtl fluid model in tapered stenosed arteries and mentioned that the velocity profiles decreases with an increase in Prandtl fluid parameters, the shape and height of the stenosis. Pralhad and Schultz [12] studied the size effects on blood flow through the stenosed artery. The unsteady response of non-Newtonian blood flow through a stenosed artery in the presence of magnetic field has been investigated by Kelvin *et al.* [8] and mentioned that the flow rate has been considerably reduced by magnetic field.

The appreciable amount of attention was paid to the nanofluids research in recent years owing to their significant contributions in engineering and biomedical research. Nanoparticles are small in size and having very large surface areas. Therefore, these fluids have extreme properties like minimal blocking in flow passages, high thermal conductivity, long-term stability, and homogeneity. This in turn, these fluids have an abounding number of potential applications in peristaltic pumps for diabetic treatments, pharmacological administration mechanisms, electronics cooling, solar collectors and nuclear applications. Initially, Choi and Eastman [6] presented the concept of nanofluids for suspension of liquids containing ultra-fine particles. Philip and Shima [11] provided an overview of the important material properties that affect the thermal properties of nanofluids and novel approaches to get extremely high thermal conductivities. Akbar *et al.* [3] analysed the influence of permeable walls along with slip on the nanofluid flow through tapered arteries with stenosis. Nadeem and Ijaz [9] studied the theoretical analysis of metallic nanoparticles on blood flow through stenosed artery with permeable walls. Nadeem and Ijaz [10] demonstrated the addition of nanoparticles to the base fluid reduces the resistive impedance of blood flow through stenosed artery. Ahmed and Nadeem [1] presented the study of (C_u, T_iO_2, Al_2O_3) nanoparticles as antimicrobials of blood

flow through diseased arteries and mentioned that the transmission of axial velocity of pure fluid is substantially lower than that of nanofluid.

In the above literature the effect of bifurcation angle on the physiological properties of blood flow is ignored. The present article deals with the pulsatile blood flow as copper suspended nanofluid through a bifurcated artery with mild stenosis in the parent lumen. The variation of flow rate, impedance and shearing stress are analyzed for different values of pertinent parameters involved in physical problem.

2. Mathematical formulation

Consider the laminar, incompressible homogeneous pulsatile blood flow through a bifurcated artery with mild stenosis in the parent lumen. The arteries, forming bifurcation are assumed to be symmetric about the parent axis and has a single mild stenosis in its lumen as shown in Figure 1. Curvature is imported at the start of the lateral junction and the flow divider so that the possibility of flow separation zones (if any) can be removed. The blood is treated as a pulsatile and copper suspended nanofluid of constant density. The fluid properties, including the electrical conductivity are assumed to be constant, except for the density, so that the Boussinesq approximation can be used. Let (r, θ, z) be defined as coordinates in a cylindrical polar coordinate system where z axis is taken along the axis of the artery, while θ and r are taken along the circumferential and radial directions, respectively.

The governing equations for the conservation of mass, momentum and temperature of the pulsatile nanofluid flow can be written as

$$\rho_{nf}\left[\frac{\partial \rho}{\partial t} + \frac{\partial u}{\partial r} + \frac{u}{r} + \frac{\partial w}{\partial z}\right] = 0, \tag{2.1}$$

$$\rho_{nf}\left[\frac{\partial u}{\partial t} + u\frac{\partial u}{\partial r} + w\frac{\partial u}{\partial z}\right] = -\frac{\partial p}{\partial r} + \mu_{nf}\frac{\partial}{\partial r}\left[2\frac{\partial u}{\partial r}\right] + \mu_{nf}\frac{\partial}{\partial z}\left[2\frac{\partial u}{\partial z} + \frac{\partial w}{\partial r}\right], \tag{2.2}$$

$$\rho_{nf}\left[\frac{\partial w}{\partial t} + u\frac{\partial w}{\partial r} + w\frac{\partial w}{\partial z}\right] = -\frac{\partial p}{\partial z} + \mu_{nf}\frac{\partial}{\partial z}\left[2\frac{\partial w}{\partial z}\right] + \frac{\mu_{nf}}{r}\frac{\partial}{\partial r}\left[r\left(\frac{\partial u}{\partial z} + \frac{\partial w}{\partial r}\right)\right] + \rho_{nf}g\beta_2(T - T_0), \tag{2.3}$$

$$(\rho_{cp})_{nf}\left[\frac{\partial T}{\partial t} + u\frac{\partial T}{\partial r} + w\frac{\partial T}{\partial z}\right] = K_{nf}\left[\frac{\partial^2 T}{\partial r^2} + \frac{1}{r}\frac{\partial T}{\partial r} + \frac{\partial^2 T}{\partial z^2}\right] + Q_1, \tag{2.4}$$

where u, w are the components of velocity in radial and axial directions respectively, g represents gravitational acceleration, β_2 represents the volumetric expansion parameter, Q_1 represents the heat generation, T represents the temperature of the fluid, ρ_{nf} represents the effective density, μ_{nf} represents the effective dynamic viscosity, $(\rho_{cp})_{nf}$ represents the heat capacitance and K_{nf} represents the effective thermal conductivity, all these are defined as follows:

$$\left. \begin{array}{l} \rho_{nf} = (1-\phi)\rho_f + \phi\rho_f, \ \mu_{nf} = \frac{\mu_f}{(1-\phi)^{2.5}}, \\[2mm] (\rho_{cp})_{nf} = (1-\phi)(\rho c_p)_f + \phi(\rho c_p)_s, \ \alpha_{nf} = \frac{K_{nf}}{(\rho c_p)_{nf}}, \\[2mm] K_{nf} = K_f\left[\frac{K_s + 2K_f - 2\phi(K_f - K_s)}{K_s + 2K_f + \phi(K_f - K_s)}\right], \end{array} \right\} \tag{2.5}$$

where α_{nf} is the effective thermal diffusivity. The effective thermal conductivity in the above expression does not consider the thermal interface resistance between the nanoparticles and

the fluid, the resultant thermal conductivity is applicable only for spherical particles due to size effects. The size effect of particle and interfacial thermal resistance can be included in computing the effective thermal conductivity. If the nanoparticle thermal conductivity is more than that of the base fluid thermal conductivity, then the ratio k_f/k_s can be approximated as zero [7]. Therefore,

$$\frac{K_s + 2K_f - 2\phi(K_f - K_s)}{K_s + 2K_f + \phi(K_f - K_s)} = 1 + 3\phi.$$

The inner $R_2(z,t)$ and outer $R_1(z,t)$ walls of the bifurcated artery with mild stenosis in the parent lumen mathematically shown ([4,5])

$$R_1(z,t) = \begin{cases} aa_1(t), & 0 \le z \le d', \\ \left(a - \frac{4\epsilon}{l_0^2}(l_0(z-d') - (z-d')^2)\,a_1(t)\right), & d' \le z \le d' + l_0, \\ aa_1(t), & d' + l_0 \le z \le z_1, \\ \left(a + r_0 - \sqrt{r_0^2 - (z-z_1)^2}\right) a_1(t), & z_1 \le z \le z_2, \\ (2r_1 \sec\beta + (z-z_2)\tan\beta)\,a_1(t), & z_2 \le z \le z_{\max}, \end{cases} \quad (2.6)$$

$$R_2(z,t) = \begin{cases} 0, & 0 \le z \le z_3, \\ \left(\sqrt{(r_0')^2 - (z-z_3-r_0')^2}\right) b_1(t), & z_3 \le z \le z_3 + r_0'(1-\sin\beta), \\ (r_0' \cos\beta + z_4)\,b_1(t), & z_3 + r_0'(1-\sin\beta) \le z \le z_{\max}, \end{cases} \quad (2.7)$$

where r_1 is the radius of the daughter artery, a is the radius of the parent artery at non-stenosed portion, l_0 is the length of the stenosis at a distance d' from the origin, β is the half the bifurcation angle, ϵ represents the maximum height of the stenosis at $z = d' + l_0/2$ and $z_{\max}$ represents the finite length of the bifurcated artery under consideration, z_1 is the location of the onset of the lateral junction, z_2 is the location of the offset of the lateral junction, z_3 is the apex. These are all functions of half of the bifurcated angle and are defined as

$$z_2 = z_1 + r_0 \sin\beta, \quad z_3 = z_2 + q_1, \quad z_4 = (z - z_3 - r_0'(1-\sin\beta))\tan\beta,$$

and q_1 is a small number lies in between 0.1 and 0.5, which is for the compatibility of the geometry. The radii of curvatures for the start of lateral junction r_0 and the flow divider r_0' are given by

$$r_0 = \frac{a - 2r_1 \sec\beta}{\cos\beta - 1} \quad \text{and} \quad r_0' = \frac{(z_3 - z_2)\sin\beta}{1 - \sin\beta}, \quad (2.8)$$

where $a_1(t)$, $b_1(t)$ are

$$\left.\begin{array}{l} a_1(t) = 1 - (\cos(\omega t) - 1)k\ \exp(-k\omega t), \\ b_1(t) = \frac{1}{a_1(t)}. \end{array}\right\}$$

The corresponding boundary conditions are

$$\left.\begin{array}{l} \frac{\partial w}{\partial r} = 0,\ \frac{\partial T}{\partial r} = 0,\ \text{on } r = 0 \text{ for } 0 \le z \le z_3, \\ w = 0,\ T = 0,\ \text{on } r = R_1(z) \text{ for all } z, \\ w = 0,\ \frac{\partial T}{\partial r} = 0,\ \text{on } r = R_2(z) \text{ for } z_3 \le z \le z_{\max}, \\ w = w_0,\ \text{at initial time.} \end{array}\right\} \quad (2.9)$$
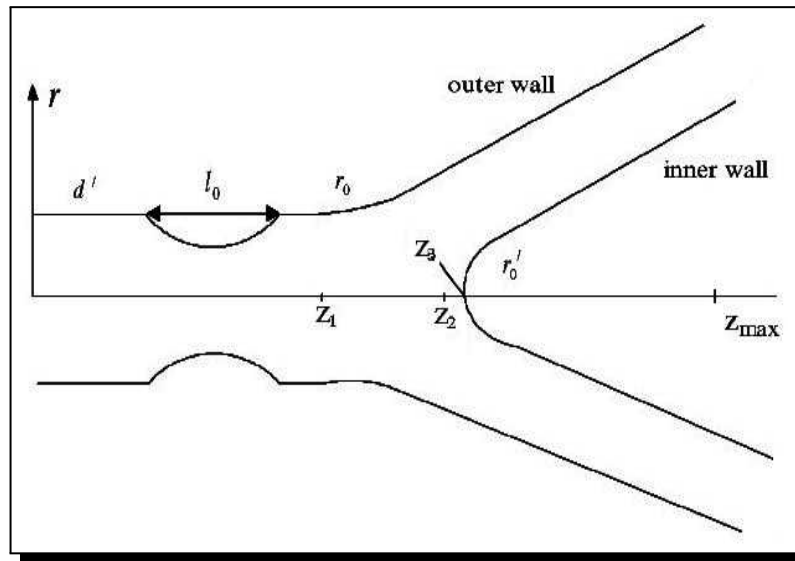
Figure 1. Schematic diagram of stenosed bifurcated artery

Since the flow is considered to be symmetric about z-axis, all the variables are independent of θ. Therefore, the velocity along a radial direction is very small and can be ignored for a low Reynolds number flow through artery with mild stenosis, this suggested that along the flow direction, the variation of all the flow attributes is taken to be zero except pressure [15]. Use the following non-dimensional variables in equations (2.1)-(2.9)

$$\left. \begin{array}{l} r = a\tilde{r}, \ u = \dfrac{aw_0\tilde{u}}{L}, \ z = L\tilde{z}, \ w = w_0\tilde{w}, \ d = L\tilde{d}, \\[2mm] P = \dfrac{Lw_0\mu_f\tilde{P}}{a^2}, \Theta = \dfrac{T}{T_w-T_0}, \ R_1(z) = a\tilde{R}_1(\tilde{z}), \ R_2(z) = a\tilde{R}_2(\tilde{z}), \ r_1 = a\tilde{r}_1, \ z_1 = a\tilde{z}_1, \ t = \dfrac{\tilde{t}}{\omega}, \end{array} \right\}$$

(2.10)

where L is serve as characteristic length and w_0 is serve as characteristic velocity.

After neglecting the tildes the equations (2.1)-(2.9) reduces to,

$$\frac{\partial p}{\partial r} = 0,$$

(2.11)

$$R_w^2 \frac{\partial w}{\partial t} = -\frac{\partial p}{\partial z} + \frac{1}{(1-\phi)^{2.5}}\left[\frac{\partial^2 w}{\partial r^2} + \frac{1}{r}\frac{\partial w}{\partial r}\right] + G_r\Theta,$$

(2.12)

$$R_w^2 P_r^2 \frac{\partial \Theta}{\partial t} = \frac{\partial^2 \Theta}{\partial r^2} + \frac{1}{r}\frac{\partial \Theta}{\partial r} + s(1+3\phi) = 0,$$

(2.13)

where $R_w^2 = \frac{\rho_{nf}\omega a^2}{\mu_f}$ is serve as the Womesley number, P_r is serve as the Prandtl number, $G_r = \frac{g\beta_2 a^2(T_w-T_0)\rho_{nf}}{w_o\mu_f}$ is serve as the Grashof number and $s = \frac{Q_1 a^2}{k_f(T_w-T_0)}$ is serve as the Heat source parameter.

The pulsatile pressure gradient represent in equation (2.12) is defined by

$$-\frac{\partial p}{\partial z} = A_0 + A_1\cos(\omega t),$$

where A_0 denotes the constant pressure gradient, A_1 denotes the amplitude of systolic and diastolic pressure component and $\omega = 2\pi f_p$, f_p represents the frequency of the pulsatile flow.

The outer and inner walls of the bifurcated artery in non-dimensional form as

$$R_1(z,t) = \begin{cases} a_1 & 0 \leq z \leq d' \\ \left(1 - \frac{4\epsilon}{al_0^2}(l_0(z-d') - (z-d')^2)\right)a_1, & d' \leq z \leq d' + l_0, \\ a_1, & d' + l_0 \leq z \leq z_1 \\ \left(1 + r_0 - \sqrt{r_0^2 - (z-z_1)^2}\right)a_1, & z_1 \leq z \leq z_2, \\ (2r_1 \sec\beta + (z-z_2)\tan\beta)a_1, & z_2 \leq z \leq z_{\max}, \end{cases}$$

$$R_2(z,t) = \begin{cases} 0, & 0 \leq z \leq z_3, \\ \left(\sqrt{(r_0')^2 - (z-z_3-r_0')^2}\right)b_1, & z_3 \leq z \leq z_3 + r_0'(1-\sin\beta), \\ (r_0'\cos\beta + z_4)b_1, & z_3 + r_0'(1-\sin\beta) \leq z \leq z_{\max}. \end{cases}$$

The boundary conditions in non-dimensional form are

$$\left.\begin{array}{l} \frac{\partial w}{\partial r} = 0, \ \frac{\partial \Theta}{\partial r} = 0, \text{ on } r = 0 \text{ for } 0 \leq z \leq z_3, \\ w = 0, \ \Theta = 0, \text{ on } r = R_1(z) \text{ for all } z, \\ w = 0, \ \frac{\partial \Theta}{\partial r} = 0, \text{ on } r = R_2(z) \text{ for } z_3 \leq z \leq z_{\max}, \\ w = w_0, \text{ at initial time.} \end{array}\right\} \quad (2.14)$$

The influence of boundaries $R_1(z,t)$ and $R_2(z,t)$ can be transferred into the governing equations and boundary conditions with the radial coordinate transformation given in [14], where $R(z,t) = R_1(z,t) - R_2(z,t)$. Therefore, equations (2.12) and (2.13), reduced the form

$$R^2 R_w^2 \frac{\partial w}{\partial t} = -R^2 \frac{dp}{dz} + \left(\frac{1}{(1-\phi)^{2.5}}\right)\frac{\partial^2 w}{\partial \xi^2}$$

$$+ \left[R R_w^2 p(k) + \frac{R}{(1-\phi)^2.5 (\xi R + R_2)}\right]\frac{\partial w}{\partial \xi} + R^2 G_r \Theta, \quad (2.15)$$

$$R^2 R_w^2 P_r^2 \frac{\partial \Theta}{\partial t} = \frac{\partial^2 \Theta}{\partial \xi^2} + \left[R R_w^2 p(k) P_r^2 + \frac{R}{(1-\phi)^2.5 (\xi R + R_2)}\right]\frac{\partial \Theta}{\partial \xi} + R^2 s (1+3\phi), \quad (2.16)$$

where $p(k) = \frac{\partial R}{\partial t} + \xi \frac{\partial R_2}{\partial t}$ is corresponding to wall motion.

The corresponding boundary conditions in transformed coordinate system are

$$\left.\begin{array}{l} \frac{\partial w}{\partial \xi} = 0, \ \frac{\partial \Theta}{\partial \xi} = 0, \text{ on } \xi = 0 \text{ for } 0 \leq z \leq z_3, \\ w = 0, \ \Theta = 0 \text{ on } \xi = 1 \text{ for all } z, \\ w = 0, \ \frac{\partial \Theta}{\partial \xi} = 0 \text{ on } \xi = 0 \text{ for } z_3 \leq z \leq z_{\max}, \\ w = w_0, \text{ at initial time.} \end{array}\right\} \quad (2.17)$$

3. Numerical Solution

The Reduced equations (2.15) and (2.16) along with the boundary conditions (2.17) are numerically solved using finite-difference scheme. A three dimensional computational grid is imposed in $z - \xi - t$ plane. The stepping process is defined by $z_i = i\Delta z$, $i = 0, 1, \cdots, N$, $\xi_j = j\Delta\xi$, $j = 0, 1, \cdots, J$ and $t_k = k\Delta t$, $k = 0, 1, \cdots, M$ where Δz, Δt and $\Delta\xi$ are step lengths along the axial, time and radial directions respectively. If $w_{i,j,k}$ and $\Theta_{i,j,k}$ represents the value of the variables w and Θ at (z_i, ξ_j, t_k) respectively, then the derivatives are replaced with equivalent central

difference approximations as given below.

$$\left.\begin{array}{l}\dfrac{\partial w}{\partial \xi}=\dfrac{1}{2}\left[\dfrac{w_{i,j+1}^{k+1}-w_{i,j-1}^{k+1}}{2\triangle \xi}+\dfrac{w_{i,j+1}^{k}-w_{i,j-1}^{k}}{2\triangle \xi}\right],\\[3mm]\dfrac{\partial^2 w}{\partial \xi^2}=\dfrac{1}{2}\left[\dfrac{w_{i,j+1}^{k+1}-2w_{i,j}^{k+1}+w_{i,j-1}^{k+1}}{(\triangle \xi)^2}+\dfrac{w_{i,j+1}^{k}-2w_{i,j}^{k}+w_{i,j-1}^{k}}{(\triangle \xi)^2}\right],\\[3mm]\dfrac{\partial w}{\partial t}=\dfrac{w_{i,j}^{k+1}-w_{i,j}^{k}}{\triangle t}.\end{array}\right\} \tag{3.1}$$

Similarly, we can write second order finite difference approximations for $\frac{\partial^2 \Theta}{\partial \xi^2}$, $\frac{\partial \Theta}{\partial \xi}$ and $\frac{\partial \Theta}{\partial t}$.

Substituting (3.1) in (2.15) and (2.16), we get the following system of equations.

$$(a_1)_{i,j}^k w_{i,j-1}^{k+1}+(a_2)_{i,j}^k w_{i,j}^{k+1}-(a_3)_{i,j}^k w_{i,j+1}^{k+1}+G_r\Theta_{i,j}^{k+1}=(r_1)_{i,j}^k, \tag{3.2}$$

$$(b_1)_{i,j}^k \Theta_{i,j-1}^{k+1}+(b_2)_{i,j}^k \Theta_{i,j}^{k+1}+(b_3)_{i,j}^k \Theta_{i,j+1}^{k+1}=(r_2)_{i,j}^k, \tag{3.3}$$

where

$$(a_1)_{i,j}^k=-\dfrac{1}{4R\triangle \xi}\left[R_w^2 p(k)+\dfrac{1}{(1-\phi)^{2.5}(\xi R+R_2)}\right]+\dfrac{1}{2R^2(\triangle \xi)^2(1-\phi)^{2.5}},$$

$$(a_2)_{i,j}^k=-\left[\dfrac{R_w^2}{\triangle t}+\dfrac{1}{R^2(\triangle \xi)^2(1-\phi)^{2.5}}\right],$$

$$(a_3)_{i,j}^k=\dfrac{1}{4R\triangle \xi}\left[R_w^2 p(k)+\dfrac{1}{(1-\phi)^{2.5}(\xi R+R_2)}\right]+\dfrac{1}{2R^2(\triangle \xi)^2(1-\phi)^{2.5}},$$

$$(r_1)_{i,j}^k=-(a_1)_{i,j}^k w_{i,j-1}^k+\left(\dfrac{1}{R^2(\triangle \xi)^2(1-\phi)^{2.5}}-\dfrac{R_w^2}{\triangle t}\right)w_{i,j}^k-(a_3)_{i,j}^k w_{i,j+1}^k+\dfrac{\partial p}{\partial z},$$

$$(b_1)_{i,j}^k=-\dfrac{1}{4R\triangle \xi}\left[\dfrac{1}{\xi R+R_2}+p(k)R_w^2 P_r^2\right]+\dfrac{1}{2R^2(\triangle \xi)^2}, \quad (b_2)_{i,j}^k=-\left[\dfrac{R_w^2 P_r^2}{\triangle t}+\dfrac{1}{R^2(\triangle \xi)^2}\right],$$

$$(b_3)_{i,j}^k=\dfrac{1}{4R\triangle \xi}\left[\dfrac{1}{\xi R+R_2}+p(k)R_w^2 P_r^2\right]+\dfrac{1}{2R^2(\triangle \xi)^2},$$

$$(r_2)_{i,j}^k=-(b_1)_{i,j}^k \Theta_{i,j-1}^k+\left[\dfrac{1}{R^2(\triangle \xi)^2}-\dfrac{p_r R_w^2}{\triangle t}\right]\Theta_{i,j}^k-(b_3)_{i,j}^k \Theta_{i,j+1}^k-s(1+3\phi).$$

The equations (3.2) and (3.3) along with the boundary conditions (2.17) are shortened into a block tridiagonal system of equations and is solved by block elimination method.

The physical quantities of interest are flow rate, impedance and shear stress for both parent and daughter arteries for different values of pertinent parameters are calculated and shown graphically.

The flow rate for both parent artery (Q_p) and daughter artery (Q_d) are obtained by

$$Q_p=2\pi R\left[R\int_0^1 \xi w\,d\xi+R_2\int_0^1 w\,d\xi\right] \tag{3.4}$$

and

$$Q_d=\pi R\left[R\int_0^1 \xi w\,d\xi+R_2\int_0^1 w\,d\xi\right]. \tag{3.5}$$

The resistance to the unidirectional blood flow (resistive impedance) in the parent artery

(λ_p) and daughter artery (λ_d) by using

$$(\lambda_p)_i = \left| \frac{z_3 \frac{dp}{dz}}{Q_p} \right|, \quad \text{for } z < z_3, \tag{3.6}$$

$$(\lambda_d)_i = \left| \frac{(z_{\max} - z_3) \frac{dp}{dz}}{Q_d} \right|, \quad \text{for } z \geq z_3. \tag{3.7}$$

The shear stress along the walls of the artery is determined by using

$$\tau = \frac{\mu_f}{(1-\phi)^{2.5}} \frac{1}{R} \frac{\partial w}{\partial \xi}. \tag{3.8}$$

4. Results and Discussions

The aim of the current study has been to investigate the flow characteristics of pulsatile blood through a stenosed bifurcated artery under the consideration that blood as copper suspended nanofluid. For the better understanding of the analysis, we have used the following data [13]: $a = 5$ mm, $d' = 10$ mm, $l_0 = 5$ mm, $\beta = \frac{\pi}{10}$, $r_1 = 0.51a$, $\epsilon = 2$, $H = 0.2$, $s = 0.2$, $\mu_f = 0.894$, $P_r = 0.7$, $R_w^2 = 1.2$, $t = 2$ sec and $G_r = 0.3$.
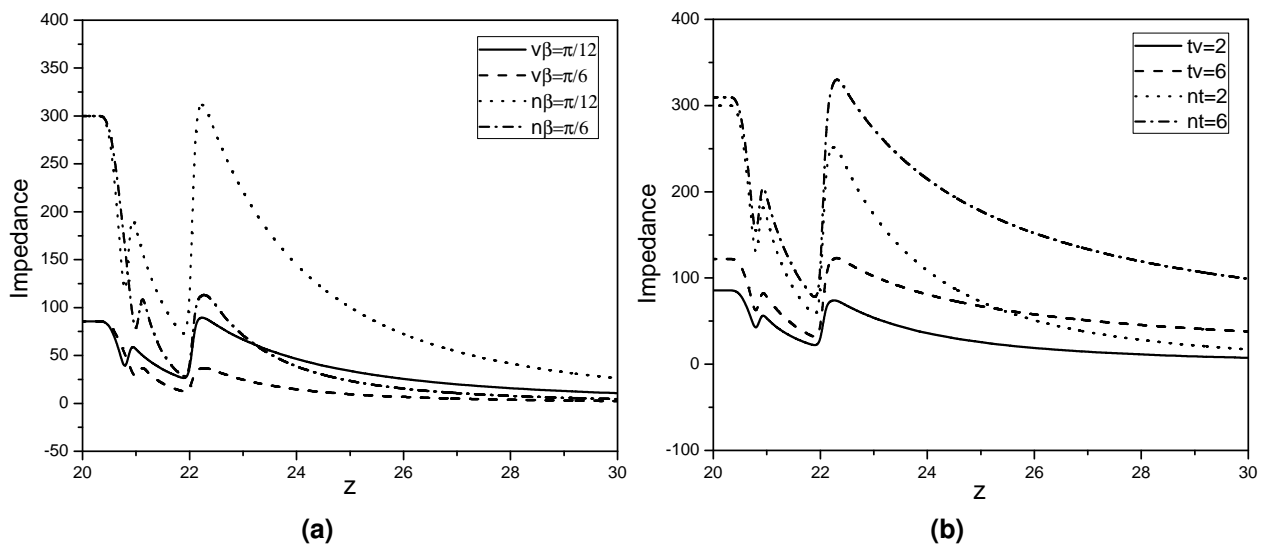
Figure 2. The effect of (a) β and (b) time t on impedance with and without nanoparticle volume fraction on both sides of the apex for fixed values of $s = 0.2$, $P_r = 0.7$, $R_w^2 = 1.2$ and $G_r = 0.3$

The influence of half of the bifurcated angle β on impedance in daughter artery with and without nanoparticle volume fraction for fixed values of $s = 0.2$, $P_r = 0.7$, $R_w^2 = 1.2$, $t = 2$ sec and $G_r = 0.3$ is presented in Figure 2a. From this figure, it is observed that impedance is decreasing with an increase in the value of β, but impedance is enhancing with an increase in the value of the nanoparticle volume fraction. The influence of time (t) on impedance with and without nanoparticle volume fraction for fixed values of $s = 0.2$, $P_r = 0.7$, $\beta = \frac{\pi}{10}$, $R_w^2 = 1.2$ and $G_r = 0.3$ near the apex is plotted in Figure 2b. It is observed that impedance increases for higher values of t on both sides of the apex. Figure 3a explores the influence of nanoparticle volume fraction on impedance with nanoparticle volume fraction for fixed values of other parameters near the

flow divider. This figure reveals that the impedance is enhanced with advanced value of ϕ on both sides of the flow divider. The influence of Womersley number R_w^2 on impedance near the apex with and without nanoparticle volume fraction is presented in Figure 3b. From this figure, it is noticed that the effect of R_w^2 is insignificant in the pure fluid, but in the case of nanofluid impedance is decreasing with increased value of R_w^2. From Figures 2a to 3b, it is to be noted that the impedance is diminishing with an advancement in the value of z, until inset of lateral junction, then a slight increase occurred suddenly, after that a gradual decrease till the apex, and again a sudden increase is observed. This is because of the divergence of the blood flow at the bifurcation of the artery. Thereafter, it is noticed that the impedance is uniform till $z_{\max}$.
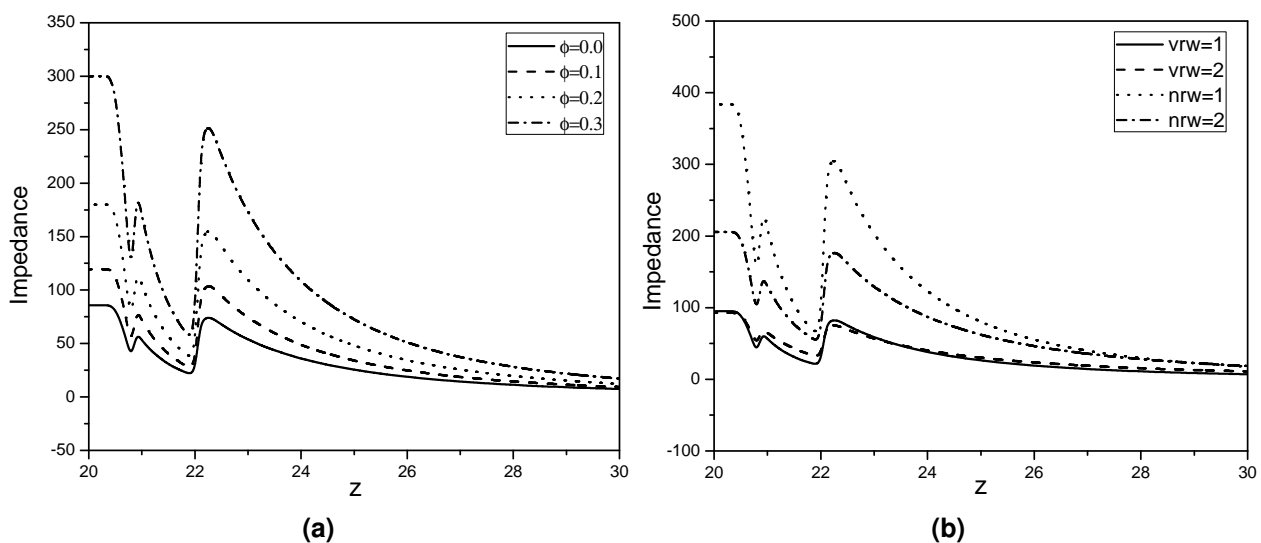
Figure 3. The influence of (a) ϕ and (b) Womersley number ($R_w^2 = 1.2$) on impedance with and without nanoparticle volume fraction on both sides of the apex for fixed values of $s = 0.2$, $P_r = 0.7$, $\beta = \frac{\pi}{10}$, $G_r = 0.3$, and time $t = 2$ sec

The variations of flow rate with β and time (t) near the apex with and without nanoparticle volume fraction for the fixed values of $s = 0.2$, $P_r = 0.7$, $R_w^2 = 1.2$ and $G_r = 0.3$ are disclosed in Figures 4a and 4b. From Figure 4a, it is observed that flow rate is increasing with an increase in the value of β while from Figure 4b flow rate is decreasing with an increase in the value of t on both sides of the apex. The variations of flow rate with nanoparticle volume fraction on both sides of the apex is plotted in Figure 5a. From this figure, it is noticed that flow rate is diminishing with an increase in the nanoparticle volume fraction on both sides of the apex, this is because of the density of the copper suspended blood is higher than that of pure blood and it slows down the blood flow which implies the decreased flow rate. The effect of the Womersley number on flow rate in both sides of the apex with and without nanoparticle volume fraction is depicted in Figure 5b. This figure reveals that the flow rate is decreasing with an increase in the values of R_w^2 and nanoparticle volume fraction on both sides of the apex. From Figures 4a and 5b, it is observed that flow rate patterns are perturbed largely near the apex in the parent artery due to the presence of backflow at the start of the lateral junction and secondary flow near the flow divider. The flow rate profiles are locally increasing till inset of the lateral junction,

then a small decrease is identified and again increase until the apex. Thereafter, these patterns found to be steady till $z_{\max}$. It is noticed that flow rate is increasing in case of pure blood as compared to copper suspended blood, because the density of the Copper suspended blood is higher than that of pure blood and it slows down the blood flow which implies the decreased flow rate.
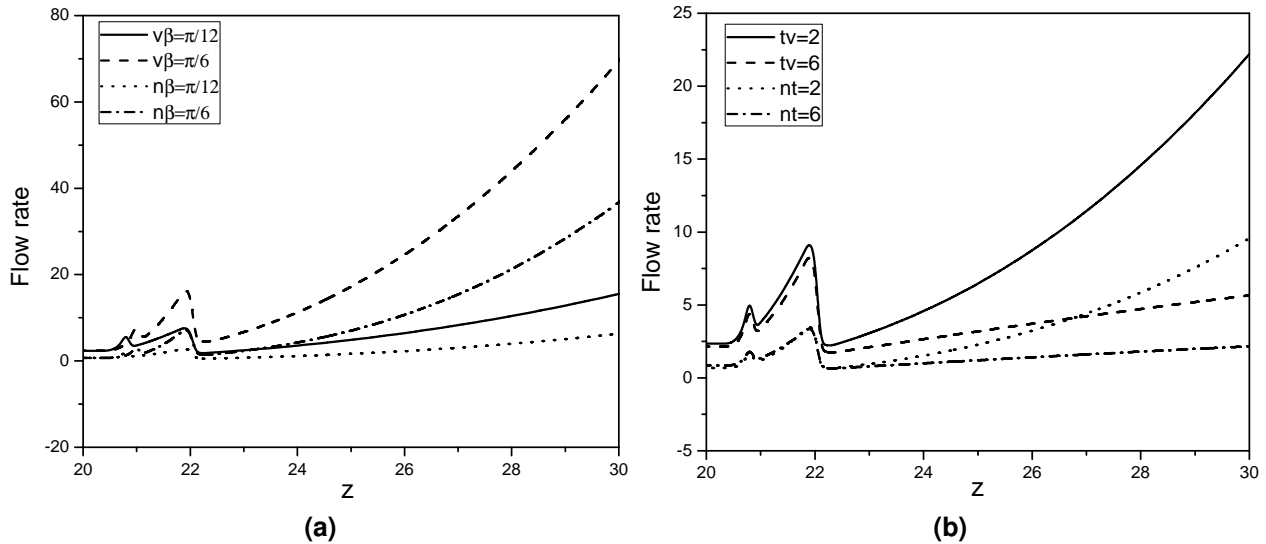
Figure 4. Variations of flow rate with (a) β and (b) time (t) with and without nanoparticle volume fraction on both sides of the apex for fixed values of $s = 0.2$, $P_r = 0.7$, $R_w^2 = 1.2$ and $G_r = 0.3$
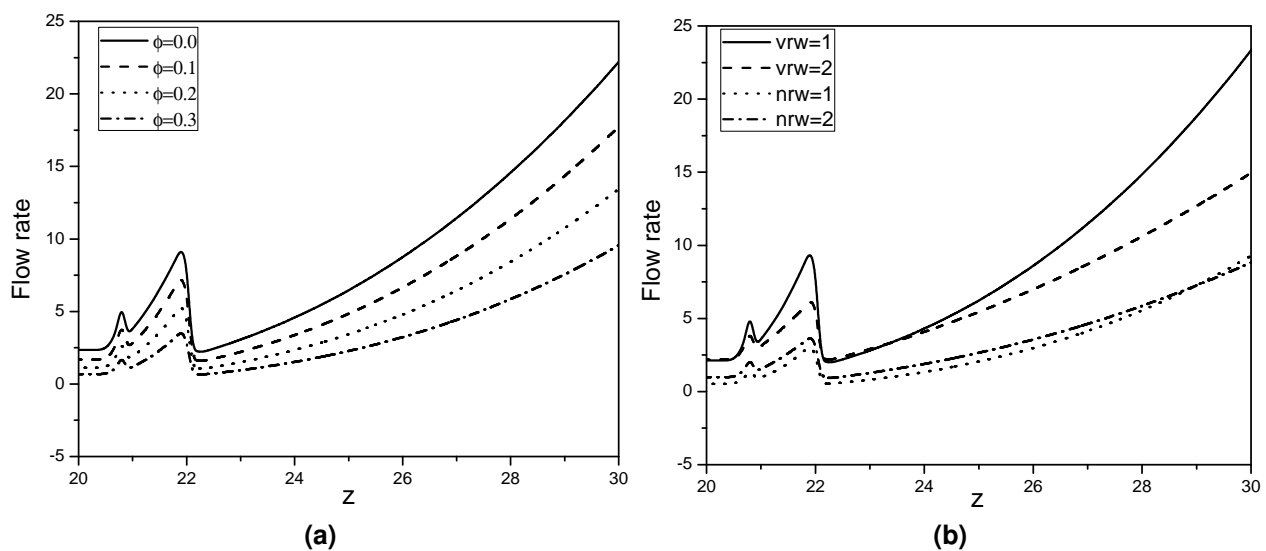
Figure 5. Effect of (a) ϕ and (b) Womersley number on flow rate with and without nanoparticle volume fraction on both sides of the apex for fixed values of $s = 0.2$, $P_r = 0.7$, $\beta = \frac{\pi}{10}$, $G_r = 0.3$ and time $t = 2$ sec

Figures 6a and 6b explore the effect of β on shear stress for fixed values of $s = 0.2$, $P_r = 0.7$, $R_w^2 = 1.2$, $t = 2$ sec and $G_r = 0.3$ along the inner and outer walls of the daughter artery with and without nanoparticle volume fraction. From Figure 6a, shear stress increases with an increase in the value of β, but it decreases for increased value of nanoparticle volume faction along the

inner wall of the daughter artery. From Figure 6b, shear stress increases with an increase in the values of β and ϕ along the outer wall of the daughter artery. The influence of t on shear stress along the inner and outer wall of the daughter artery with and without nanoparticle volume fraction for fixed values of $s = 0.2$, $P_r = 0.7$, $\beta = \frac{\pi}{10}$, $R_w^2 = 1.2$ and $G_r = 0.3$ are illustrated in Figures 7a and 7b. From these figures, it is noticed that shear stress is increasing along the inner wall and decreasing along the outer wall for higher value of t.
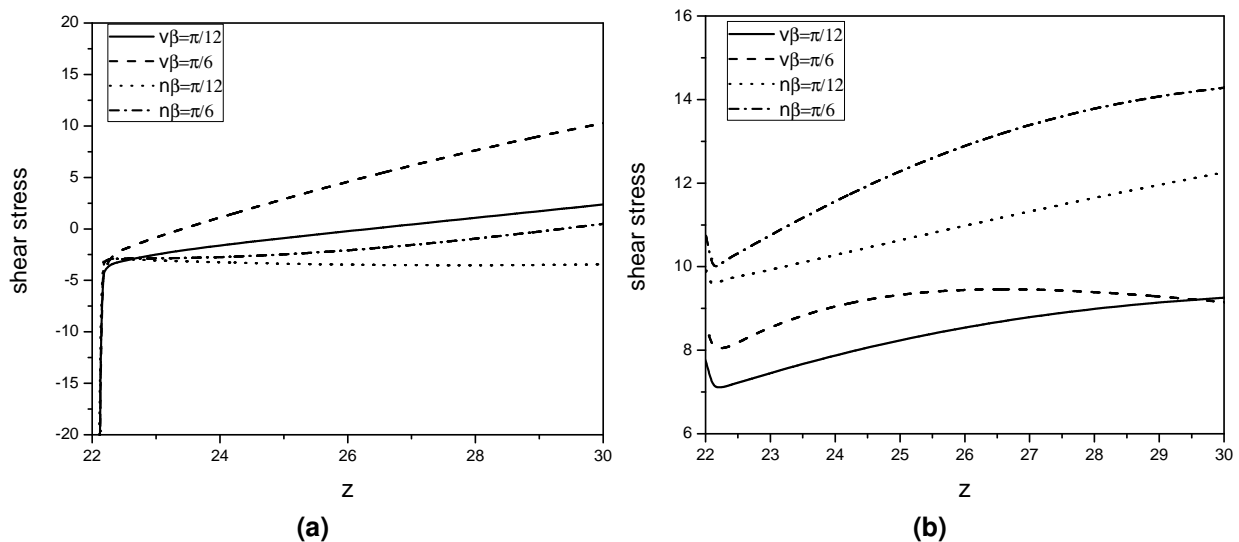
Figure 6. Effect of β on shear stress along the (a) inner and (b) outer walls of the daughter artery with and without nanoparticles volume fraction for fixed values of $s = 0.2$, $P_r = 0.7$, $R_w^2 = 1.2$, $G_r = 0.3$ and time $t = 2$ sec
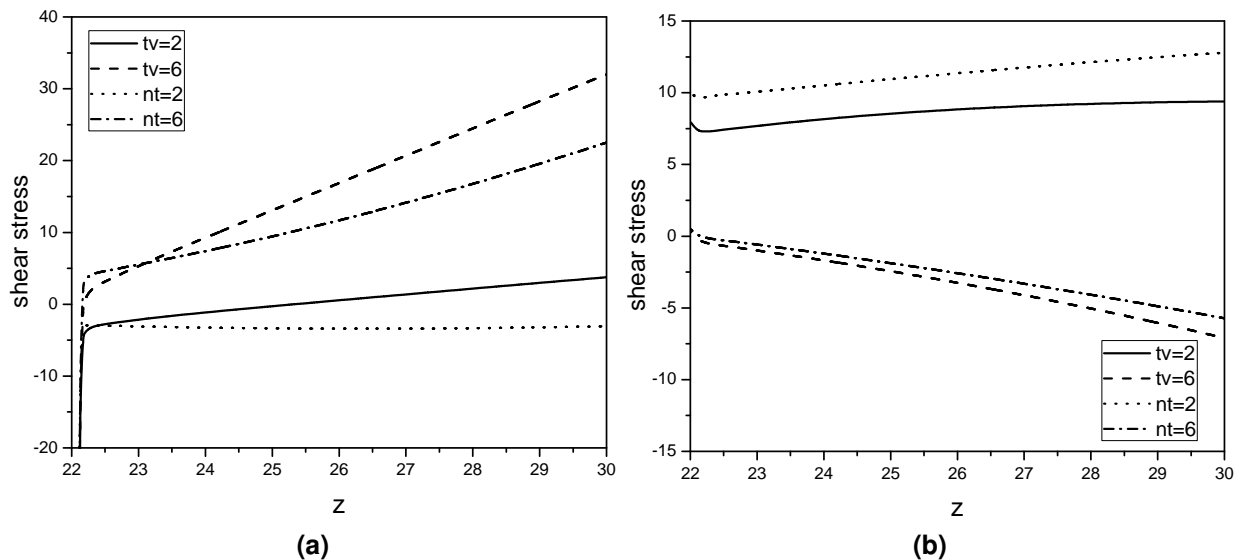
Figure 7. Influence of $time(t)$ on shear stress along the (a) inner and (b) outer walls of the daughter artery with and without nanoparticles volume fraction for fixed values of $s = 0.2$, $P_r = 0.7$, $R_w^2 = 1.2$ and $G_r = 0.3$

The influence of ϕ on shear stress along the inner and outer wall of the daughter artery for fixed values of $s = 0.2$, $P_r = 0.7$, $\beta = \frac{\pi}{10}$, $R_w^2 = 1.2$, $G_r = 0.3$ and time $t = 2$ sec are presented in Figures 8a and 8b. From these figures, it is concluded that shear stress is decreasing along the inner wall and increasing along the outer wall of the daughter artery with an increase in the value of ϕ. The variations of shear stress with Womersley number along the inner and outer walls of the daughter artery with and without nanoparticle volume fraction for fixed value of other parameters are shown in Figures 9a and 9b. From these figures shear stress is rising along the inner wall and falling along the outer wall of the daughter artery with an increase in the value of Womersley number.
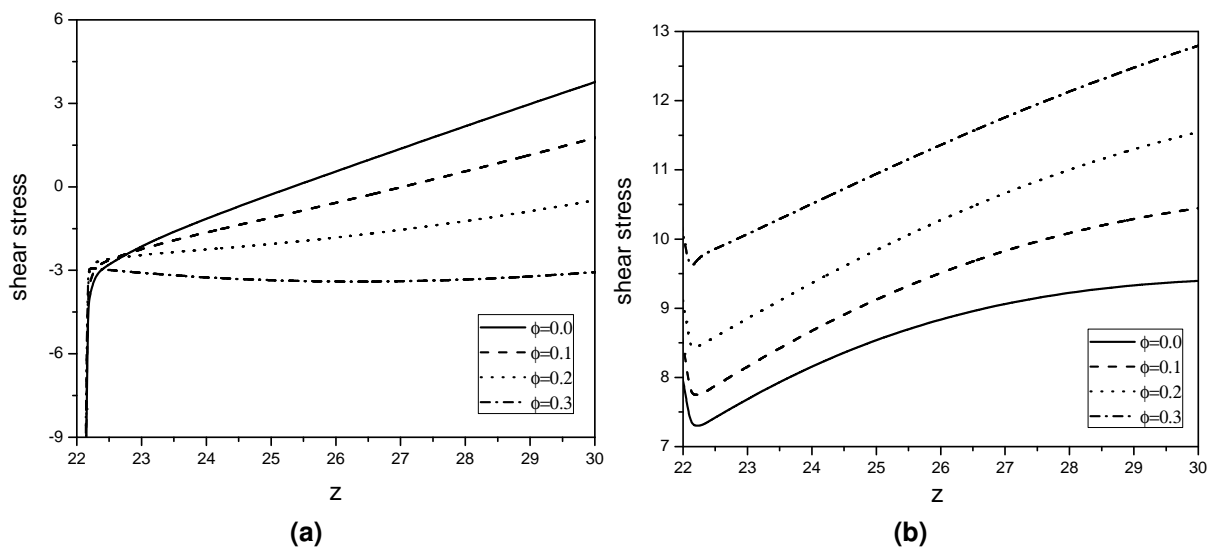
Figure 8. Variations of shear stress with ϕ along (a) the inner and (b) the outer walls of the daughter artery with and without nanoparticles volume fraction for fixed values of $s = 0.2$, $P_r = 0.7$, $\beta = \frac{\pi}{10}$, $R_w^2 = 1.2$, $G_r = 0.3$ and time $t = 2$ sec
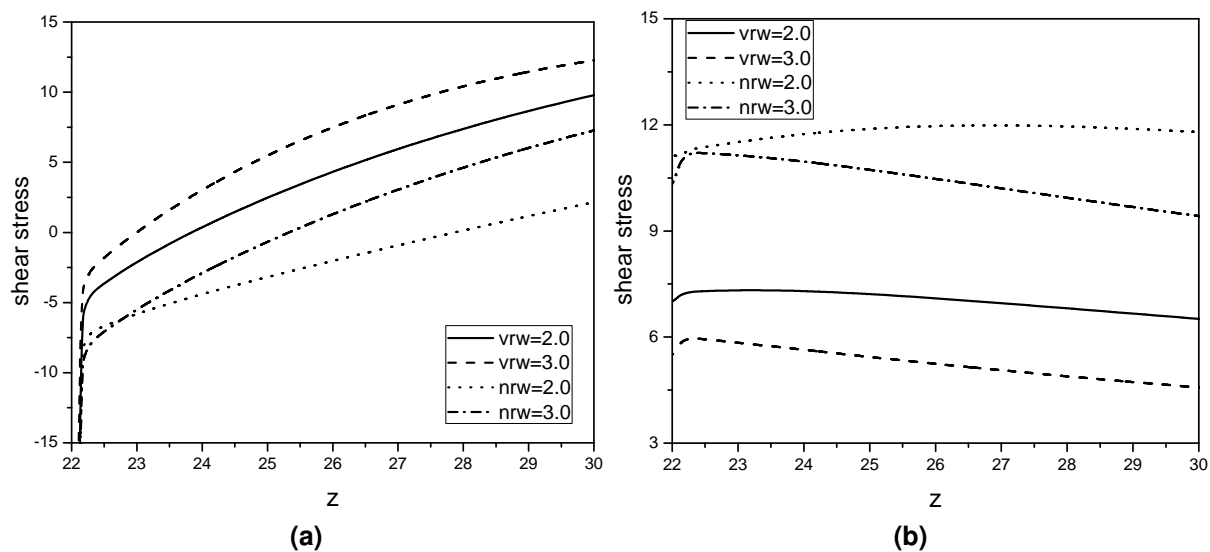
Figure 9. Effect of R_w on shear stress along (a) the inner and (b) the outer walls of the daughter artery with and without nanoparticles volume fraction for fixed values of $s = 0.2$, $P_r = 0.7$, $\beta = \frac{\pi}{10}$, $G_r = 0.3$ and time $t = 2$ sec

Figures 10a and 10b explore the effect of heat source parameter (s) on shear stress along the inner and outer wall of the daughter artery with and without nanoparticle volume fraction for fixed values of $P_r = 0.7$, $\beta = \frac{\pi}{10}$, $R_w^2 = 1.2$, $G_r = 0.3$ and time $t = 2$ sec. The effect of s is almost negligible on shear stress along the inner and outer wall of the daughter artery. It is observed from Figures 6 to 10 that shear stress is decreasing along the inner wall and increasing along the outer wall for increased value of the nanoparticle volume fraction.
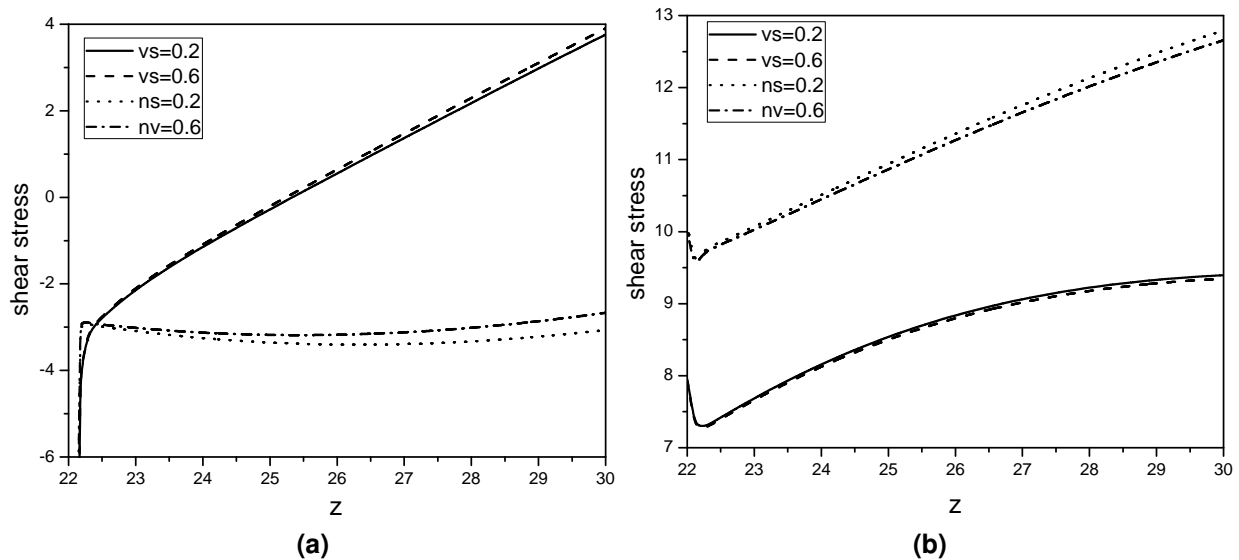
Figure 10. Variations of shear stress with s along (a) the inner and (b) the outer walls of the daughter artery with and without nanoparticles volume fraction for fixed values of $s = 0.2$, $P_r = 0.7$, $\beta = \frac{\pi}{10}$, $R_w^2 = 1.2$, $G_r = 0.3$ and time $t = 2$ sec
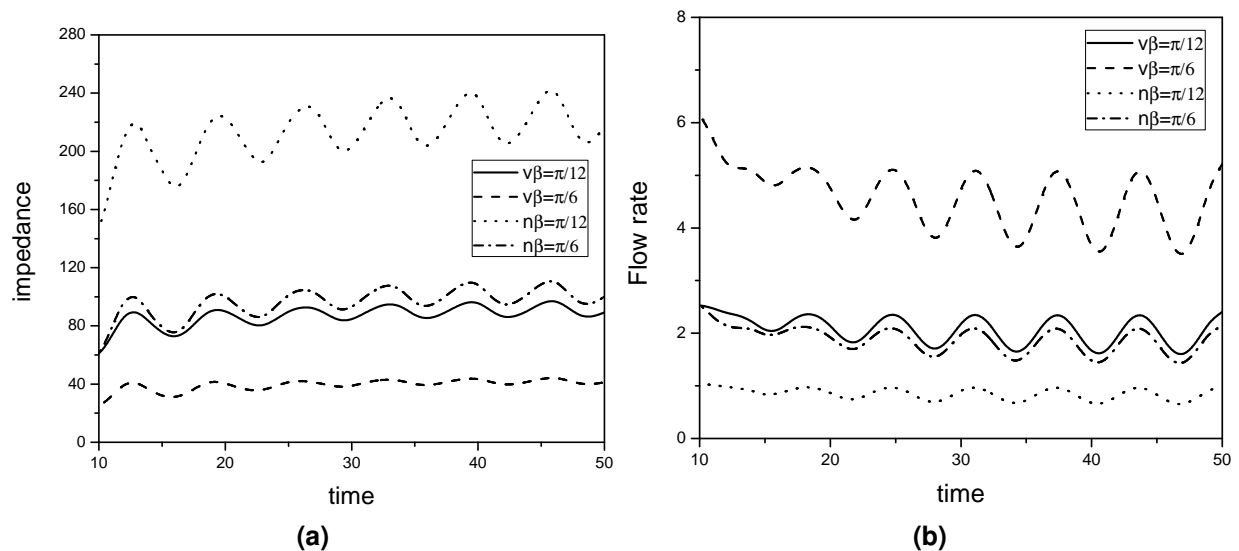
Figure 11. Effect of β on (a) impedance and (b) flow rate against time in daughter artery with and without nanoparticles volume fraction for fixed values of $s = 0.2$, $P_r = 0.7$, $G_r = 0.3$ and $R_w^2 = 1.2$

The effect of β on impedance and flow rate against time in daughter artery with and without nanoparticles volume fraction for fixed values of $s = 0.2$, $P_r = 0.7$, $G_r = 0.3$ and $R_w^2 = 1.2$ are

depicted in Figures 11a and 11b respectively. From these figure, it is noticed that impedance is diminishing (Figure 11a) and flow rate is enhancing (Figure 11b) with increase in the value of β in daughter artery. Figures 12a and 12b explore the influence of R_w^2 on impedance and flow rate against time in daughter artery with and without nanoparticles volume fraction for fixed values of $s = 0.2$, $P_r = 0.7$, $G_r = 0.3$ and $\beta = \frac{\pi}{10}$. From these figures, it is clear that impedance and flow rate are increasing in half period and decreasing in another half period for increase in the value of R_w^2. From Figures 12 and 13, it is worth to mention that impedance is rising and flow rate is falling in the daughter artery with increase in the value of nanoparticle volume fraction.
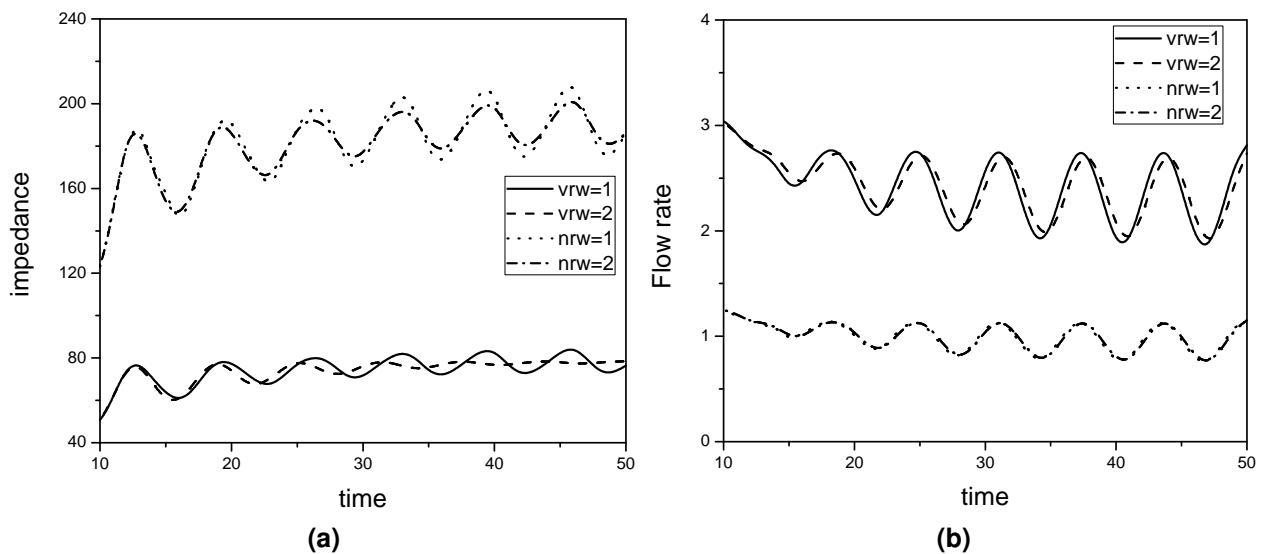
Figure 12. Influence of R_w^2 on (a) impedance and (b) flow rate against time in daughter artery with and without nanoparticles volume fraction for fixed values of $s = 0.2$, $P_r = 0.7$, $G_r = 0.3$ and $\beta = \frac{\pi}{10}$
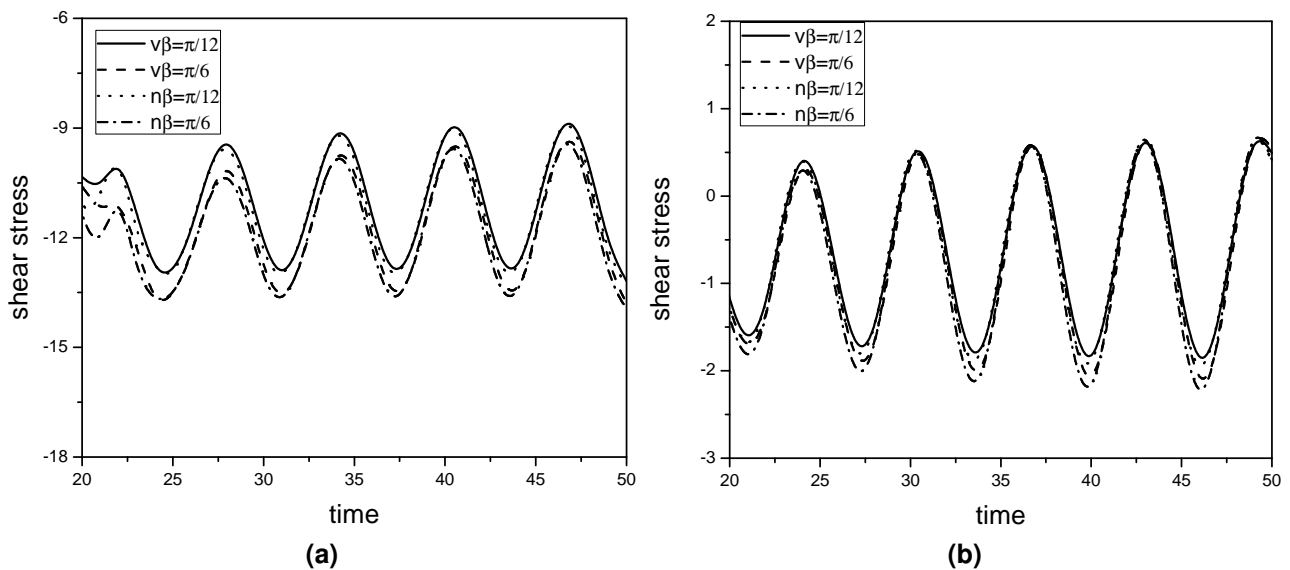
Figure 13. Effect of β on shear stress along (a) the inner and (b) the outer walls of the daughter artery against time with and without nanoparticles volume fraction for fixed values of $s = 0.2$, $P_r = 0.7$, $R_w^2 = 1.2$, $G_r = 0.3$

The influence of β on shear stress along the inner and the outer walls of the daughter artery against time with and without nanoparticles volume fraction for fixed values of $s = 0.2$, $P_r = 0.7$, $R_w^2 = 1.2$, $G_r = 0.3$ are presented in Figures 13a and 13b. From these figures, it is observed that shear stress is decreasing along the inner and outer walls of the daughter artery with and without nanoparticle volume fraction.

(a)

(b)
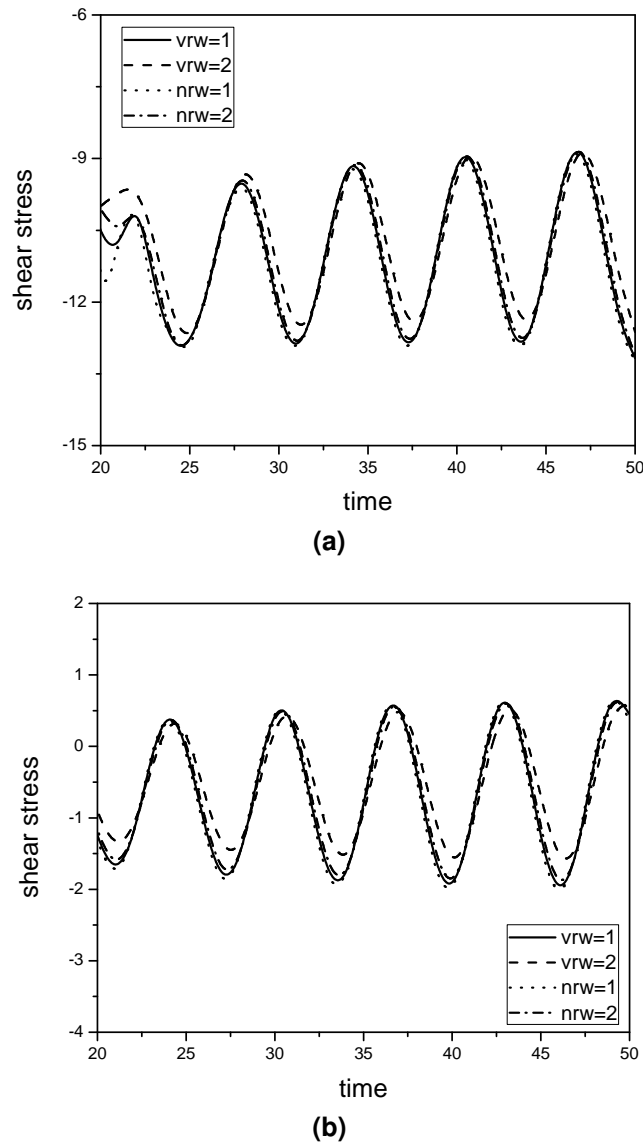
Figure 14. Influence of R_w^2 on shear stress along (a) the inner and (b) the outer walls of the daughter artery against time with and without nanoparticles volume fraction for fixed values of $s = 0.2$, $P_r = 0.7$, $\beta = \frac{\pi}{10}$, $G_r = 0.3$

The influence of R_w^2 on shear stress along the inner and outer walls of the daughter artery against time with and without nanoparticles volume fraction for fixed values of $s = 0.2$, $P_r = 0.7$, $\beta = \frac{\pi}{10}$, $G_r = 0.3$ are shown in Figures 14a and 14b. From these figures, it is recognized that shear stress is decreasing in half cycle and increasing in another half cycle along the inner and outer walls of the daughter artery with and without nanoparticle volume fraction.

5. Conclusions

The present study reveals and concludes the following points. The influence of β, ϕ and s on copper suspended blood as a nanofluid flow through a bifurcated artery with mild stenosis in the parent lumen. Applications of heat transfer are producing the variations in temperature of the object which is helpful for the purpose of thermal therapy in the treatment of tumor, glands etc.

- The impedance has been increasing with an increase in the value of ϕ, R_w, t and decrease in the value of β on both sides of the apex.

- The flow rate has been increasing with an increase in the value of β and decrease in the value of ϕ, R_w, t on both sides of the apex.

- The shear stress has been increasing with an increase in the values of β, R_w, t and s and decrease with an advancement in the value of ϕ along the inner wall of the daughter artery. But, along the outer wall of the daughter artery shear stress increases with an increase in the value of ϕ and it decrease with an increase in the value of β, R_w, t, s.

Competing Interests

The authors declare that they have no competing interests.

Authors' Contributions

All the authors contributed significantly in writing this article. The authors read and approved the final manuscript.

References

[1] A. Ahmed and S. Nadeem, The study of (C_u, T_iO_2, Al_2O_3) nanoparticles as antimicrobials of blood flow through diseased arteries, *Journal of Molecular Liquids* **216** (2016), 615 – 623, DOI: 10.1016/j.molliq.2016.01.059.

[2] N. S. Akbar, Blood flow analysis of Prandtl fluid model in tapered stenosed arteries, *Ain Shams Engineering Journal* **5** (2014), 1267 – 1275, DOI: 10.1016/j.asej.2014.04.014.

[3] N. S. Akbar, S. U. Rahman, R. Ellahi and S. Nadeem, Nano fluid flow in tapering stenosed arteries with permeable walls, *International Journal of Thermal Sciences* **85** (2014), 54 – 61, DOI: 10.1016/j.ijthermalsci.2014.06.009.

[4] S. Chakravarty, P. K. Mandal and A. Mandal, Mathematical model of pulsatile blood flow in a distensible aortic bifurcation subject to body acceleration, *International Journal of Engineering Science* **38** (2000), 215 – 238, DOI: 10.1016/S0020-7225(99)00022-1.

[5] S. Chakravarty and S. Sen, A mathematical model of blood flow in a catheterized artery with a stenosis, *Journal of Mechanics in Medicine and Biology* **9** (2009), 377 – 392, DOI: 10.1142/S0219519409002985.

[6] S. U. S. Choi and J. A. Eastman, Enhancing thermal conductivity of fluids with nanoparticles, *The Proceedings of the 1995 International Mechanical Engineering Congress and Exposition*, San Francisco, USA, FED 231/MD 66, 99 – 105 (1995), URL: `https://www.osti.gov/servlets/purl/196525`.

[7] J. Garg, B. Poudel, M. Chiesa, J. B. Gordon, J. J. Ma, J. B. Wang, R. F. Ren, Y. T. Kang, H. Ohtani, J. Nanda, G. H. McKinley and G. Chen, Enhanced thermal conductivity and viscosity of copper nanoparticles in ethylene glycol nanofluid, *Journal of Applied Physics* **103** (2008), 074301 – 074306, DOI: 10.1063/1.2902483.

[8] Md. A. Ikbal, S. Chakravarty, K. K. L. Wong, J. Mazumdar and P. K. Mandala, Unsteady response of non-Newtonian blood flow through a stenosed artery in magnetic field, *Journal of Computational and Applied Mathematics* **230** (2009), 243 – 259, DOI: 10.1016/j.cam.2008.11.010.

[9] S. Nadeem and S. Ijaz, Theoretical analysis of metallic nanoparticles on blood flow through stenosed artery with permeable walls, *Physics Letters A* **379** (2015), 542 – 554, DOI: 10.1016/j.physleta.2014.12.013.

[10] S. Nadeem and S. Ijaz, Theoretical examination of nanoparticles as a drug carrier with slip effects on the wall of stenosed arteries, *International Journal of Heat and Mass Transfer* **93** (2016), 1137 – 1149, DOI: 10.1016/j.ijheatmasstransfer.2015.10.041.

[11] J. Philip and P. D. Shima, Thermal properties of nanofluids, *Advances in Colloid and Interface Science* **183-184** (2012), 30 – 45, DOI: 10.1016/j.cis.2012.08.001.

[12] R. N. Pralhad and D. H. Schultz, Modeling of arterial stenosis and its applications to blood diseases, *Mathematical Biosciences* **190** (2004), 203 – 220, DOI: 10.1016/j.mbs.2004.01.009.

[13] S. Shaw, R. S. R. Gorla, P. V. S. N. Murthy and C.-O. Ng, Pulsatile casson fluid flow through a stenosed bifurcated artery, *International Journal of Fluid Mechanics Research* **36**(1) (2009), 43 – 63, DOI: 10.1615/InterJFluidMechRes.v36.i1.30.

[14] G. C. Shit and M. Roy, Pulsatile flow and heat transfer of a magneto-micropolar fluid through a stenosed artery under the influence of body acceleration, *Journal of Mechanics in Medicine and Biology* **11** (2011), 643 – 661, DOI: 10.1142/S0219519411003909.

[15] D. Srinivasacharya and D. Srikanth, Flow of micropolar fluid through catheterized artery — A mathematical model, *International Journal of Biomathematics* **5**(2) (2012), 1250019-1 – 1250019-12, DOI: 10.1142/S1793524511001611.

[16] D. F. Young, Effect of a time-dependent stenosis on flow through a tube, *Journal of Manufacturing Science and Engineering* **90** (1968), 248 – 254, DOI: 10.1115/1.3604621.